IEEE Photonics Journal
An IEEE Photonics Society Publication

Open Access

Photonic Crystal Fiber Temperature Sensor Based on Coupling Between Liquid-Core Mode and Defect Mode

Volume 7, Number 2, April 2015

Qiang Liu
Shuguang Li
Hailiang Chen, Student Member, IEEE
Zhenkai Fan
Jianshe Li

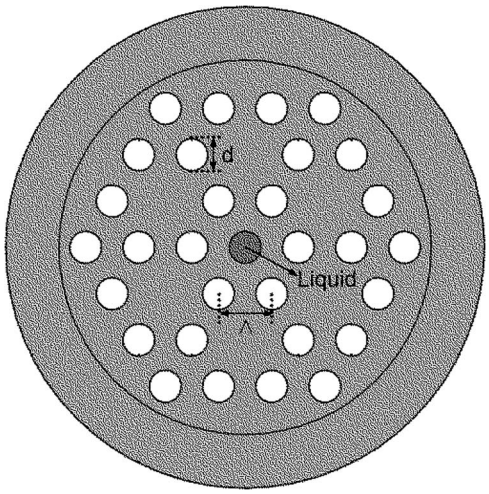

DOI: 10.1109/JPHOT.2015.2404911
1943-0655

IEEE photonics SOCIETY

IEEE

Photonic Crystal Fiber Temperature Sensor Based on Coupling Between Liquid-Core Mode and Defect Mode

Qiang Liu, Shuguang Li, Hailiang Chen, *Student Member, IEEE*, Zhenkai Fan, and Jianshe Li

Key Laboratory of Metastable Materials Science and Technology, College of Science, Yanshan University, Qinhuangdao 066004, China

DOI: 10.1109/JPHOT.2015.2404911

Manuscript received February 4, 2015; revised February 12, 2015; accepted February 12, 2015. Date of publication February 24, 2015; date of current version March 2, 2015. This work was supported in part by the National Natural Science Foundation of China under Grant 61178026 and Grant 61475134 and in part by the Natural Science Foundation of Hebei Province of China under Grant E2012203035. Corresponding author: S. Li (e-mail: shuguangli@ysu.edu.cn).

Abstract: A high-sensitivity temperature sensor of compact photonic crystal fiber (PCF) based on the coupling between liquid-core mode and defect mode has been analyzed by the finite element method. The temperature sensitive materials with high refractive index ($n = 1.65$ at 25 °C), which support liquid-core modes, are filled into the central air hole of PCF. Six cores are formed by removing air holes in the second layer. The six cores work as defect modes and show high confinement losses. The liquid-core mode couples to defect mode as the phase matching condition is satisfied. The sensitivity and figure of merit reach −1.85 nm/°C, −0.072/°C and −1.95 nm/°C, −0.035/°C. The temperature sensor is competitive in the reported temperature sensors. The simple structure is easy to fabricate, and the structure can be further improved.

Index Terms: Photonic crystal fiber, temperature sensor.

1. Introduction

In the temperature sensor field, optical temperature sensor shows a promising direction which shows many advantages such as high sensitivity, large temperature detecting range, stability, and so on. Fiber-optic temperature sensors are the most popular. Chen [1] reported a fiber Bragg grating sensor with sensitivity of 10.47 pm/°C, where the temperature changed from 0 °C to 140 °C. Pang [2] reported a fiber-optic temperature sensor with sensitivity of 240 pm/°C based on the theory of leaky mode resonance from fiber core to outer cladding, where the temperature changed from −20 °C to 80 °C. Wu [3] reported a optical fiber temperature sensor based on the principle of fiber loop mirror with the sensitivities of 0.8833 nm/°C and 0.7896 nm/°C, where the temperature detecting windows were about 10 °C and 20 °C, respectively. Geng [4] proposed a temperature sensor based on photonic crystal fiber (PCF) Mach-Zehnder interferometer and the sensitivity of −1.83 nm/°C was realized, where the temperature detecting window was about 35 °C. Peng [5] proposed a temperature sensor of PCF based on surface plasmon resonance and the sensitivity as high as 720 pm/°C was obtained, where the temperature changed from 0 °C to 100 °C. Srivastava [6] demonstrated a temperature sensor with sensitivity of 70 pm/°C based on photonic crystal waveguide with metal layer, where the

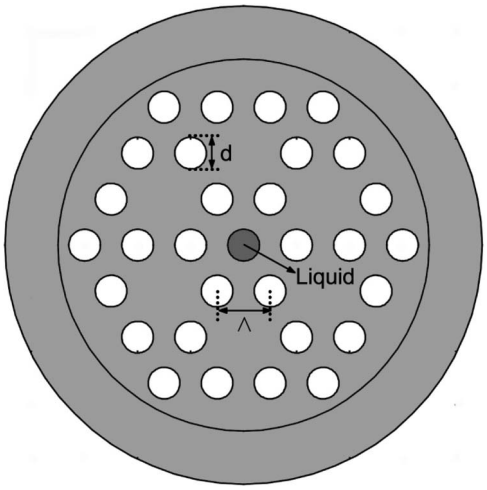

Fig. 1. Cross section of the proposed temperature sensor based on PCF. The temperature sensitive material is filled into the central hole of PCF.

temperature varied from 0 °C to 527 °C. Ju [7] demonstrated a temperature sensor based on PCF and the sensitivity reached to 0.147 rad/°C, where the temperature varied from 20 °C to 120 °C. An optical fiber temperature sensor based on colloidal quantum dot luminescence was demonstrated based on the colloidal-core PCF with the sensitivity of 70 pm/°C, where the temperature detecting window is 85 °C [8]. A compact temperature sensor based on fiber loop mirror combined with an alcohol-filled high-birefringence PCF was proposed and the sensitivity reached to 6.6 nm/°C, but the temperature detecting window was just 14 °C [9]. An ultrasensitive temperature sensing device was demonstrated based on the light coupling between the fundamental core mode and the fundamental rod mode in the satellite waveguide, and the sensitivity could reach to 54.3 nm/°C, but the temperature detecting window was just 1.4 °C [10]. A sensitivity of 2.58 nm/°C was achieved based on PCF Sagnac interferometer, where the temperature detecting window was 17 °C [11].

In this paper, we design a temperature sensor based on the coupling between liquid-core mode and defect mode by the finite element method. We assume to inject the temperature sensitive materials of high refractive index into the central air hole of PCF to form a liquid core which supports liquid-core mode. The six air holes in the second layer are removed to form six cores which support defect mode. As the phase matching condition is satisfied, the coupling between liquid-core mode and defect mode happens. This temperature detecting windows are 60 °C better than [3], [4], [9]–[11], and the sensitivities are −1.85 nm/°C and −1.95 nm/°C better than [1]–[6], [8]. Our temperature sensor, showing high sensitivity, high linearity, and high figure of merit (FOM), is competitive in the reported temperature sensors.

2. Structure Designed and Simulation Method

The cross section of the proposed fiber sensor is shown in Fig. 1. The air holes are arranged in a triangular lattice. The lattice pitch is $\Lambda = 2\ \mu$m. The diameters of all the air holes are $d = 1.2\ \mu$m. The background material of the fiber is fused silica whose dispersion relationship corresponding to temperature is calculated by the Sellmeier equation [12]:

$$n^2(\lambda, T) = (1.31552 + 6.90754 \times 10^{-6}T) + \frac{(0.788404 + 23.5835 \times 10^{-6}T)\lambda^2}{\lambda^2 - (0.0110199 + 0.584758 \times 10^{-6}T)} + \frac{(0.91316 + 0.548368 \times 10^{-6}T)\lambda^2}{\lambda^2 - 100} \quad (1)$$

where λ is the free space wavelength in microns, and T is the temperature in Celsius. The existing forms of silica are crystalline and amorphous. If the arrangement of silica is ordered, the

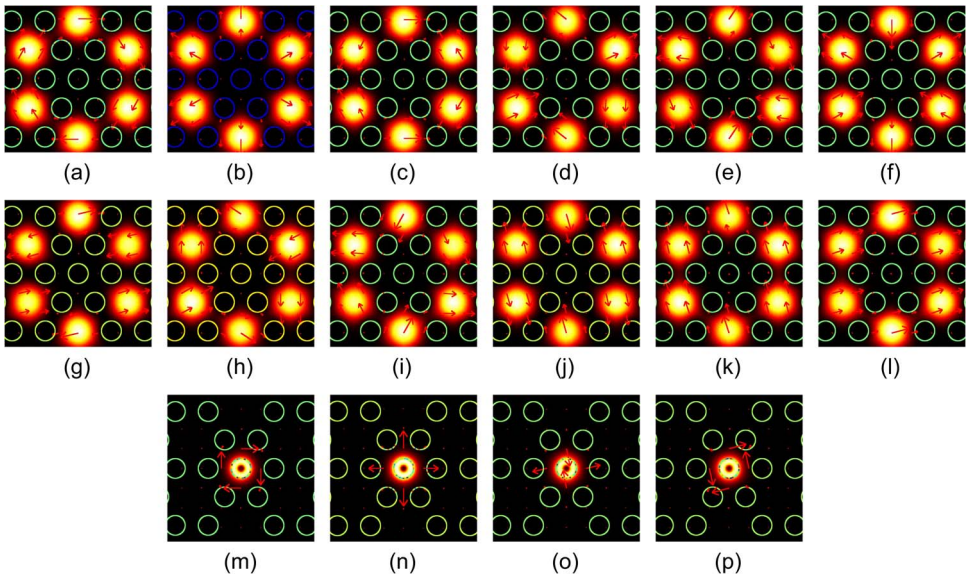

Fig. 2. Electric field distributions of (a)–(l) defect modes and (m)–(p) liquid-core modes. The arrow represents the direction of the electric field. The coupling between defect mode is shown in (a) and liquid-core mode shown in (m), defect mode shown in (b), and liquid-core mode shown in (n) is employed to analyze for our temperature sensor, respectively.

form is crystalline. If the arrangement of silica is not ordered, the form is amorphous. Continuous heating and slow cooling will form crystalline silica. If the cooling is too fast, molecules of silica can not rearrange in the role of bonds. Then, the form of the silica will be amorphous. The melting temperature of silica is about 1670 °C, but the temperature detecting range is just from 20 °C to 80 °C. The form of the fiber drawn is crystalline. As low detecting temperature cannot melt the fiber, the amorphous nature of the fiber will not interfere with temperature detection. The six cores in the second layer are formed by removing air holes and support defect mode which is shown in Fig. 2(a)–(l). The arrow represents the direction of the electric field. The temperature sensitive liquids [13] filled into the central air hole of PCF has a refractive index of 1.65 at room temperature (25 °C). Its refractive index is tunable between 20 °C and 80 °C with a temperature coefficient of $dn/dT = -0.000465/^{\circ}\mathrm{C}$. The liquid-core mode shown in Fig. 2(m)–(p) is similar to mode in holey fiber. The arrow represents the direction of the electric field. Its mode can be controlled by liquid material. Nowadays, the fabrication techniques include extrusion, cast rod in tube, ultrasonic drilling and stacking for the perform of PCF. The selective infiltration of PCF can be achieved by the fs laser-assisted infiltration procedure. First, one end of the PCF is fully blocked with a section of single-mode fiber. Second, the central air hole is opened via subsequent fs laser drilling. Finally, the liquid can be filled into the central hole by capillary effect [10]. All the modes in the PCF are leaky modes because the real part of refractive index is lower than background material. The losses of liquid-core mode and defect mode will be changed by filling different temperature sensitive materials. The effective refractive index of liquid-core mode will be affected more than defect mode by changing the liquid materials. For our temperature sensor, the coupling between liquid-core mode in Fig. 2(m) and (n) and defect mode in Fig. 2(a) and (b) is employed.

Finite element method is used to study the real part and imaginary part of effective refractive index in PCF by the software of Comsol Multiphysics. Perfectly Matched Layer (PML) is used to absorb radiant energy and not reflect energy. Cylindrical coordinate is used for PML to absorb the radiant energy from fiber axis. The outer boundary of PML is set to be scattering boundary condition to further reduce reflecting energy. The computation area is discretized into triangular sub-domains whose number in our structure is 6802.

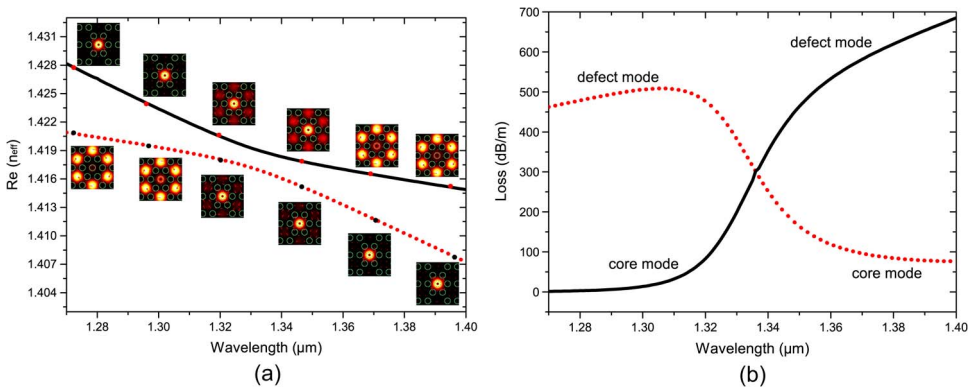

Fig. 3. (a) Real part of mode refractive index and (b) loss as a function of wavelength when a complete coupling happens. The insets in (a) show electric field distributions of the coupled modes at the selected wavelengths. For the black solid curve in (b), the loss follows liquid-core mode at the shorter wavelength and follows defect mode at the longer wavelength. For the red dot curve in (b), the loss follows defect mode at the shorter wavelength and follows liquid-core mode at the longer wavelength.

3. Numerical Results

At first, the coupling between liquid-core mode in Fig. 2(m) and defect mode in Fig. 2(a) is analyzed to understand the properties of mode coupling. Fig. 3 shows the real part of refractive index and loss dependence on the operating wavelength λ when the temperature is 50 °C. The loss is calculated by

$$\alpha(x, y) = 8.686 \times \frac{2\pi}{\lambda} \mathrm{Im}(n_{\mathrm{eff}}) \times 10^6 \tag{2}$$

where unit of the loss and wavelength is dB/m and micrometers, respectively, and Im(n_{eff}) represents the imaginary part of effective refractive index of mode. The illustrations of mode field distributions are shown in Fig. 3(a). For the upper mode, the mode field is mainly distributed in liquid core at the shorter wavelength, mode field begins to transfer from liquid core to outer cores as wavelength increases, the energies of liquid-core mode and defect mode are equal at the turning of the curve, and almost all the field transfers from liquid core to outer cores at the longer wavelength. For the lower mode, the mode transition is contrary to that of the upper mode. For the black solid cure in Fig. 3(b), the loss follows liquid-core mode at the shorter wavelength, and follows defect mode at the longer wavelength. The losses of liquid-core mode and defect mode are equal at the intersection of black solid cure and red dot cure. The intersection corresponds to the tuning of the curve in Fig. 3(a). This is called complete coupling. The coupling between liquid-core mode in Fig. 2(n) and defect mode in Fig. 2(b) is the same as this. In the following, the coupling between liquid-core mode and defect mode is always complete coupling.

Then, we use coupled-mode theory [14], [15] to explain the above phenomena. For liquid-core mode and defect mode, the coupled-mode equations are

$$\frac{dE_1}{dz} = i\beta_1 E_1 + i\kappa E_2 \tag{3}$$

$$\frac{dE_2}{dz} = i\kappa E_1 + i\beta_2 E_2 \tag{4}$$

where β_1 and β_2 are the propagation constants of liquid-core mode and defect mode, E_1 and E_2 are the mode fields of the two modes, κ is the coupling strength, and z is the propagation

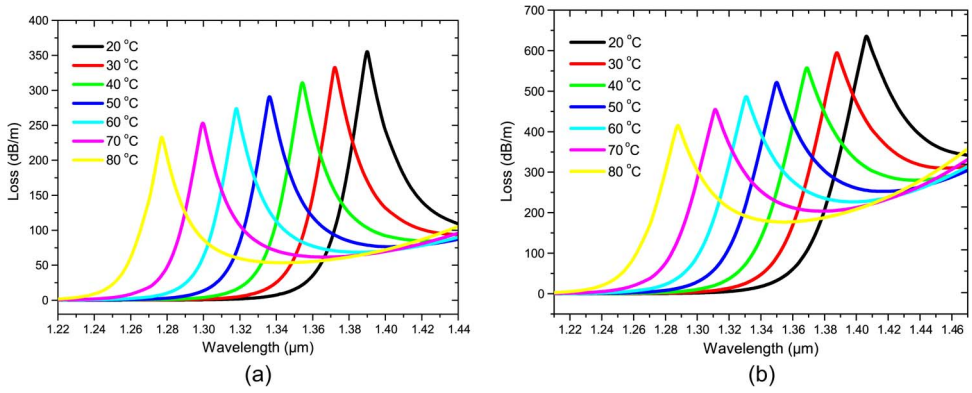

Fig. 4. Loss spectra for (a) the liquid-core mode shown by Fig. 2(m) and (b) the liquid-core mode shown by Fig. 2(n) as a function of wavelength with the temperature changing from 20 °C to 80 °C.

length. We assume the propagation constant of the coupling mode to be β. Then, E_1 and E_2 can be assumed to be the following equations:

$$E_1 = Aexp(i\beta z) \tag{5}$$

$$E_2 = Bexp(i\beta z). \tag{6}$$

Equations (5) and (6) are substituted into (3) and (4), and we can get β

$$\beta_{\pm} = \beta_{ave} \pm \sqrt{\delta^2 + \kappa^2} \tag{7}$$

where $\beta_{ave} = (\beta_1 + \beta_2)/2$, and $\delta = (\beta_1 - \beta_2)/2$. The two modes are leaky because their real parts of mode refractive index are lower than those of the background materials. For leaky modes, β_1 and β_2 are complex. Therefore, δ can be represented by $\delta = \delta_r + i\delta_i$. The real parts of propagation constants of liquid-core mode and defect mode are equal as phase matching condition is satisfied, so $\delta_r = 0$. Then, we get

$$\delta^2 + \kappa^2 = -\delta_i^2 + \kappa^2 \tag{8}$$

where, when $\delta_i < \kappa$, the real parts of β_+ and β_- are different, the imaginary parts of β_+ and β_- are equal, a complete coupling happens. When $\delta_i > \kappa$, the real parts of β_+ and β_- are equal, the imaginary parts of β_+ and β_- are different, a incomplete coupling happens. The incomplete coupling has been analyzed by us in [16]. In the following, the coupling between liquid-core mode and defect mode is always complete coupling.

As temperature increases, the refractive indices of temperature sensitive materials decrease. The refractive indices of liquid-core modes decrease, while the refractive indices of defect modes don't have significant variation. By this way, the phase matching points will change. Fig. 4 shows the loss spectra for (a) liquid-core mode shown in Fig. 2(m) and (b) liquid-core mode shown in Fig. 2(n) dependence on the operating wavelength λ with the temperature changing from 20 °C to 80 °C. The intensities of losses at the phase matching points decrease as temperature increasing. Fig. 5 shows the wavelengths at the phase matching points for (a) liquid-core mode shown in Fig. 2(m) and (b) liquid-core mode shown in Fig. 2(n) dependence on temperature. Sensitivity of the temperature sensor can be calculated by

$$S = \frac{d\lambda_{peak}}{dT}. \tag{9}$$

For the liquid-core mode shown by Fig. 2(m), the λ_{peak} is 1300 nm at the temperature 70 °C and drops to 1277 nm at the temperature 80 °C. The estimated sensitivity is $S = (1300 - 1277)/(70 - 80) = -2.3$ nm/°C. The fitting cure of λ_{peak} dependence on temperature is shown in

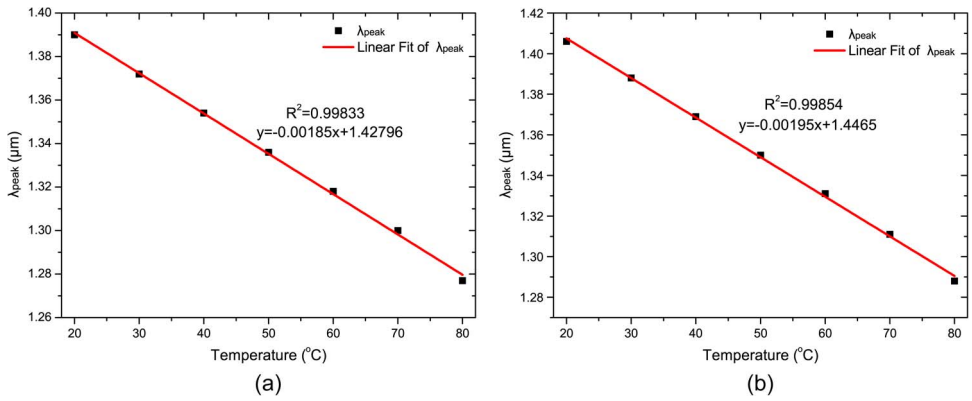

Fig. 5. Resonance wavelength for (a) the liquid-core mode shown by Fig. 2(m) and (b) the liquid-core mode shown by Fig. 2(n) as a function of temperature.

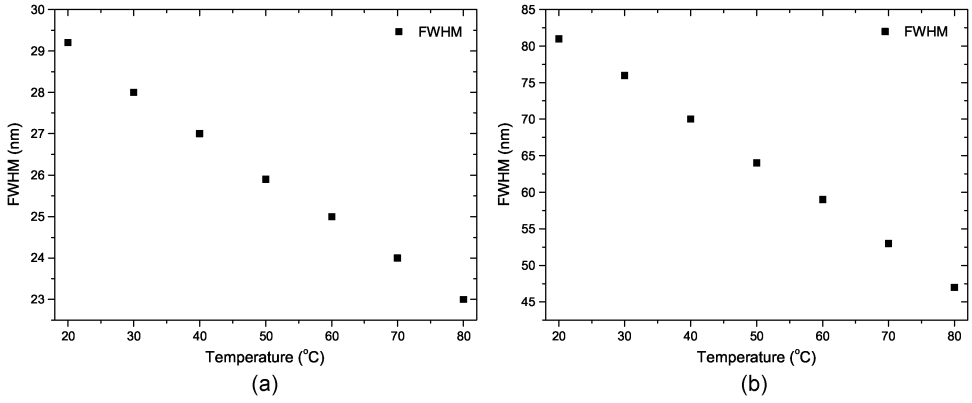

Fig. 6. FWHM for (a) the liquid-core mode shown by Fig. 2(m) and (b) the liquid-core mode shown by Fig. 2(n) as a function of temperature.

Fig. 5. The average sensitivity can reach to -1.85 nm/°C and -1.95 nm/°C. The high linearity can reach to 0.99833 and 0.99854 better than 0.9799 in [3] which is important in the actual application for sensor.

The spectra width and signal to noise ratio (SNR) are also significant for sensor which can be demonstrated by figure of merit (FOM). FOM is calculated by

$$\text{FOM} = \frac{S}{\text{FWHM}} \tag{10}$$

where FWHM expresses the full width at half-maximum of spectra. Fig. 6 shows FWHM increases as temperature decreases. This is mainly because the resonance wavelength red shifts as temperature decreases, the proportion of material loss in the total loss increases and the proportion of coupling loss in the total loss decreases.} The average FOM is $-0.072/^{\circ}$C and $-0.035/^{\circ}$C better than $0.026/^{\circ}$C in [5] and 0.023 in [6].

Fig. 7 shows the schematic of the temperature sensor system. The left standard single-mode fiber (SMF) is used to connect light source and PCF. The light source is stable, continuous and broadband light. And it will be coupled to liquid core of PCF through SMF. The right standard SMF is used to connect optical spectrum analyzer (OSA) and PCF. The light from liquid core of PCF will be coupled to SMF. The PCF is putted into temperature control chamber to adjust temperature. The background material of the SMF and PCF is silica. The single material of silica is

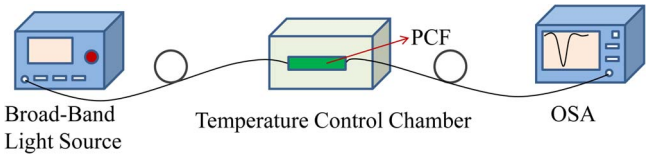

Fig. 7. Schematic of the temperature sensor system. The left SMF is used to connect light source and PCF. The right standard SMF is used to connect OSA and PCF. The PCF is put into temperature control chamber to adjust temperature.

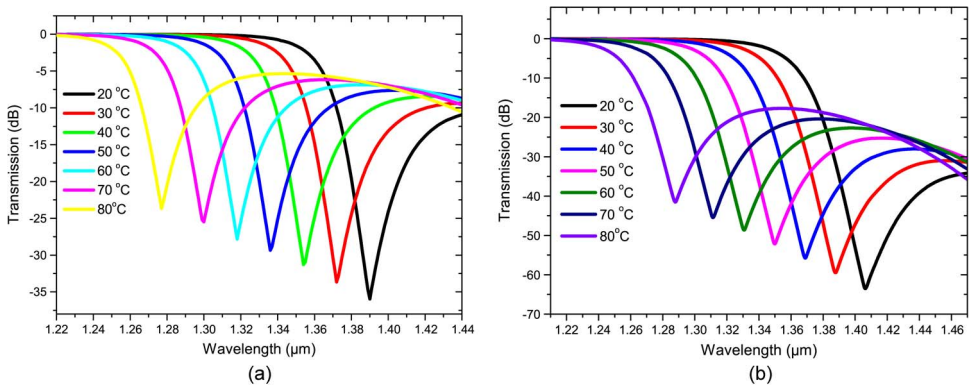

Fig. 8. Transmittance for (a) the liquid-core mode shown by Fig. 2(m) and (b) the liquid-core mode shown by Fig. 2(n) as a function of wavelength.

not sensitive to temperature and the sensitivity is just 25 pm/°C [12]. The influence of the SMF material on temperature can be ignored. In realistic conditions, we only need to consider the effect of PCF filled with temperature sensitive material on temperature. Because of the short length of the PCF, it is easy to make the tiny fiber have a uniform temperature. In addition, silica is not active chemically and it is not easy to react with water and most acids in the actual applications. Fig. 8 shows the transmittance dependence on operating wavelength λ with temperature changing from 20 °C to 80 °C. The fiber length is assumed to be 100 mm. The output power is calculated by

$$P_{\text{out}} = P_{\text{in}} \exp\left(\frac{-\alpha L}{4.343}\right). \tag{11}$$

L is the fiber length. The transmittance is obtained by

$$T_r = 10\log_{10}\left(\frac{P_{\text{out}}}{P_{\text{in}}}\right). \tag{12}$$

Dip wavelength blue shifts from 1390 nm to 1277 nm for (a) liquid-core mode shown by Fig. 2 (m) and shifts from 1406 nm to 1288 nm for (b) liquid-core mode shown by Fig. 2(n) as temperature increases and the transmittance increases at the same time.

Finally, the tolerance of realistic fabrication are considered. We calculate the impacts of the slight changes of the diameters of all the holes on the loss spectrum. Fig. 9 shows the loss spectrum for the liquid-core mode shown by the Fig. 2(m) as temperature is 50 °C or 60 °C and the diameters of all the holes of PCF fluctuate 12 nm. The numerical results show that loss spectrum red shift as the diameters of the holes increase, but the sensitivity is nearly the same. The characteristics of transmission spectrum should be measured in the laboratory for the drawn PCF with liquid before using it in the realistic situation, because the air hole size of drawn PCF may have a certain error compared with the simulation model.

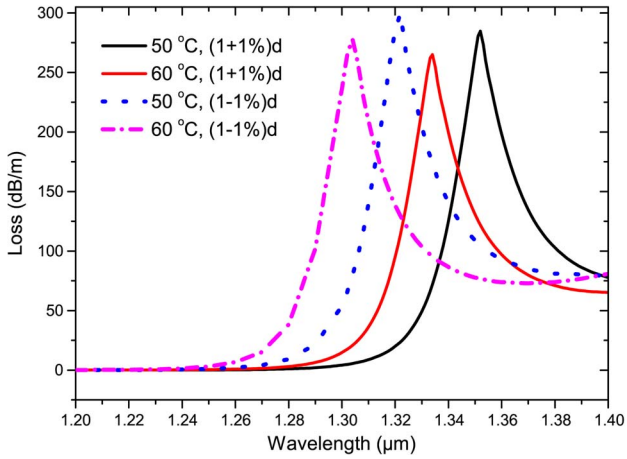

Fig. 9. Loss spectrum as structural deformation is considered.

4. Conclusion

A high-sensitivity temperature sensor based on compact PCF is proposed by the finite element method. A temperature-sensitivity material is injected into the central air hole of PCF and supports liquid-core mode. The six cores in the second layer are formed by removing air holes and work as defect mode. As phase matching condition is satisfied, the liquid-core mode couples to defect mode completely and reveals loss peak which is employed to detect temperature. The sensor shows high sensitivity, high linearity, and nice FOM. Our temperature sensor of simple structure is competitive in the temperature sensor field and suitable to measure temperature in reality. The structure can be further optimized to obtain better results.

Acknowledgement

The authors would like to thank the anonymous reviewers for their valuable comments that improved the work presented in this paper.

References

[1] C. Chen *et al.*, "Sensitivity of photonic crystal fiber modes to temperature, strain and external refractive index," *Opt. Exp.*, vol. 16, no. 13, pp. 9645–9653, Jun. 2008.
[2] F. Pang *et al.*, "Special optical fiber for temperature sensing based on cladding-mode resonance," *Opt. Exp.*, vol. 16, no. 17, pp. 12 967–12 972, Aug. 2008.
[3] D. Wu, Y. Zhao, and H. Hu, "Experimental research on FLM temperature sensor with an ethanol-filled photonic crystal fiber," *Sens. Actuators A, Phys.*, vol. 209, pp. 62–67, Jan. 2014.
[4] Y. Geng, X. Li, X. Tan, Y. Deng, and X. Hong, "Compact and ultrasensitive temperature sensor with a fully liquid-filled photonic crystal fiber Mach–Zehnder interferometer," *IEEE Sens. J.*, vol. 14, no. 1, pp. 167–170, Jan. 2014.
[5] Y. Peng, J. Hou, Z. Huang, and Q. Lu, "Temperature sensor based on surface plasmon resonance within selectively coated photonic crystal fiber," *Appl. Opt.*, vol. 51, no. 26, pp. 6361–6367, Sep. 2012.
[6] T. Srivastava, R. Das, and R. Jha, "Highly sensitive plasmonic temperature sensor based on photonic crystal surface plasmon waveguide," *Plasmonics*, vol. 8, pp. 515–521, Aug. 2012.
[7] J. Ju, Z. Wang, W. Jin, and M. Demokan, "Temperature sensitivity of a two-mode photonic crystal fiber interferometric sensor," *IEEE, Photon. Technol. Lett.*, vol. 18, no. 20, pp. 2168–2170, Oct. 2006.
[8] A. Bozolan, R. M. Gerosa, C. J. S. Matos, and M. A. Romero, "Temperature sensing using colloidal-core photonic crystal fiber," *IEEE Sens. J.*, vol. 12, no. 1, pp. 195–200, Jan. 2012.
[9] W. Qian *et al.*, "High-sensitivity temperature sensor based on an alcohol-filled photonic crystal fiber loop mirror," *Opt. Lett.*, vol. 36, no. 9, pp. 1548–1550, May 2011.
[10] Y. Wang, M. Yang, D. N. Wang, and C. R. Liao, "Selectively infiltrated photonic crystal fiber with ultrahigh temperature sensitivity," *IEEE Photon. Technol. Lett.*, vol. 23, no. 20, pp. 1520–1522, Oct. 2011.
[11] Y. Cui *et al.*, "Temperature sensor by using selectively filled photonic crystal fiber Sagnac interferometer," *IEEE Photon. J.*, vol. 4, no. 5, pp. 1801–1808, Feb. 2012.
[12] G. Ghosh, M. Endo, M. Endo, and T. Iwasaki, "Temperature-dependent Sellmeier coefficients and chromatic dispersions for some optical fiber glass," *J. Lightw. Technol.*, vol. 12, no. 8, pp. 1338–1342, Aug. 1994.

[13] J. Du *et al.*, "Thermally tunable dual-core photonic bandgap fiber based on the infusion of a temperature-responsive liquid," *Opt. Exp.*, vol. 16, no. 6, pp. 4263–4269, Mar. 2008.
[14] Z. Zhang, Y. Shi, B. Bian, and J. Lu, "Dependence of leaky mode coupling on loss in photonic crystal fiber with hybrid cladding," *Opt. Exp.*, vol. 16, no. 3, pp. 1915–1922, Jan. 2008.
[15] L. Chen *et al.*, "Design for a single-polarization photonic crystal fiber wavelength splitter based on hybrid-surface plasmon resonance," *IEEE Photon. J.*, vol. 6, no. 4, Aug. 2014, Art. ID. 2200909.
[16] Q. Liu, S. Li, and H. Chen, "Two kinds of polarization filter based on photonic crystal fiber with nanoscale gold film," *IEEE Photon. J.*, vol. 7, no. 1, Feb. 2015, Art. ID. 2700210.